Asian Journal of Chemistry; Vol. 35, No. 2 (2023), 352-360

ASIAN JOURNAL OF CHEMISTRY

https://doi.org/10.14233/ajchem.2023.26879

Silk Protein Hydrolysate for Corrosion Mitigation of Mild Steel in 1 N H_2SO_4

V. NIJARUBINI, J. MALLIKA*, and M. MANTHARASALAN

Department of Chemistry, PSG College of Arts and Science, Coimbatore-641014, India

*Corresponding author: E-mail: mallika@psgcas.ac.in

Received: 24 October 2022; *Accepted*: 15 November 2022; *Published online*: 30 January 2023; AJC-21116

In view as corrosion inhibitor, silk protein hydrolysate (SPH), a water-soluble hydrolysate obtained from silk protein (biopolymer) exhibits excellent protection to mild steel in 1 N H_2SO_4, especially at low concentration levels. Weight loss analysis propose a maximum efficiency for 10 ppm SPH at 303 K. Potentiodynamic polarization measurement revealed its functioning as a mixed-type inhibitor with enhanced polarization resistance. The best fits observed with Langmuir isotherm suggested the inhibitor-metal interaction to occur *via* physisorption mechanism. Surface examination through SEM (EDXS), water contact angle, AFM, FT-IR and Raman spectroscopy confirmed the formation of protective film.

Keywords: Silk protein hydrolysate, Corrosion, Mild steel, Physisorption, Protective film.

INTRODUCTION

Mild steel finds extensive usage in the modern world for its low cost, easy availability and demanding properties like high ductility, malleability and excellent mechanical resistance [1,2]. The major and the most common issue faced by industries while using mild steel is its propensity to corrosion as strong acids are used for cleaning/descaling/rust removal operations [3,4]. This leads to the metal destruction and reduces the life-span of materials. Several approaches are in lieu to repress corrosion in the acidic environment [5,6]. Traditional methods involve the use of organic inhibitors containing P, S, O and N gets adsorbed on the metal surface and protects metals in the aggressive environment. However, organic compounds are difficult to synthesize and also have remarkable impact on the environment. The economic and environmental considerations prompted the researches to step forward in search of biocompatible material and numerous findings are reported over the decades, using plant extracts [7-11], amino acids [12,13], proteins [14,15] and biopolymers [16-18].

Several researches reported that amino acids and protein are more than likely involved as corrosion inhibitors [19]. Roy *et al.* [20] reported the effective corrosion performance of gluten hydrolysate on mild steel in 1 N HCl, whereas El Ibrahimi *et al.* [21] reported the inhibition performance of hydrolyzed lignin towards mild steel corrosion in HCl medium. Such studies provoked an interest to investigate the anti-corrosion performance of silk protein hydrolysate. Silk is a proteinous fiber produced by silkworms in the form of cocoon. The fiber consists of 70-80% of water insoluble fibroin and 20-30% of water soluble sericin [22,23]. Fibroin acts as the structural component of silk and sericin acts as glue holding the fibroin filaments together. The hydrolysis of silk proteins breaks down the complex peptide chains to lower molecular weights. In present study, commercially available silk protein hydrolysate was investigated for its adsorption characteristics and corrosion inhibition performance on mild steel in 1 N H_2SO_4 using non-electrochemical, electrochemical methods and surface analysis techniques.

EXPERIMENTAL

Mild steel sheets of composition C- 0.069, Si- 0.077, Mn- 0.29, S- 0.014, Cr-0.011, Cu- 0.007, Al- 0.01 and Fe in balance (wt.%) were shaped into rectangular samples of dimension 3 cm × 1 cm × 0.1 cm. The metal plates were polished to mirror finish using different grades of silicon carbide grits, thereafter washed thoroughly with double distilled water, degreased with ethanol, dried and stored in desiccator before use.

The inhibitor, silk protein hydrolysate (SPH) purchased from Suboneyo Pharmaceuticals was used without any further

modification. HPLC analysis of SPH listed the presence of different amino acids *viz.* aspartic acid, glutamic acid, serine, glycine, tyrosine, valine, methionine, tryptophan, isoleucine, phenylalanine, leucine and lysine. AR grade 98% sulphuric acid and double distilled water were used to prepare 1 N H_2SO_4 solution of volume 100 mL comprising of 1, 2, 4, 8 and 10 ppm concentrations of the inhibitor.

Weight loss method: The pretreated samples were accurately weighed and dipped in 1 N H_2SO_4 in absence and presence of different inhibitor concentrations for immersion time (1, 2, 3, 6, 12 and 24 h) at 303 K. Whereas, the duration of investigation was optimized to 1 h for 313, 323 and 333 K. The metal specimens retrieved from the medium after appropriate duration were cleaned with water, acetone, dried and re-weighed. From the pre- and post-weight of metal substrates the corrosion rate (CR) and inhibition efficiency (IE) values were calculated by using eqn. 1 and 2, repectively [24,25]:

$$\text{Corrosion rate (mmpy)} = \frac{87.6 \times W}{\rho A t} \quad (1)$$

where W is the weight loss of mild steel (g), ρ is the density of the mild steel (g cm^{-3}), A is the area of the metal (cm^2), t is the exposure time (h).

$$IE\ (\%) = \frac{W_a - W_b}{W_a} \times 100 \quad (2)$$

where W_a and W_b corresponds to the weight loss values in the absence and presence of inhibitor.

Electrochemical studies: The potentiodynamic polarization studies were carried out at 303 K in a traditional three-electrode system. Mild steel surface sealed in resin with an exposed area of 0.3 cm^2 was used as working electrode. Prior to use, the uncovered surface was polished with a series of emery sheets of different grades and then washed with double distilled water, dried and stored in desiccator. Saturated calomel electrode, platinum electrode were employed as counter and reference electrode. Preceding the electrochemical investigation, the working electrode was immersed in the test medium to achieve steady state open-circuit potential. The polarization studies were carried out at a sweeping potential of ± 0.25 mV with regard to the open circuit potential at a scan rate of 0.01 Vs^{-1}. The Tafel curves in the cathodic and anodic regions were extrapolated to corrosion potential to get corrosion current densities (i_{corr}), corrosion potential (E_{corr}) and the slopes of the anodic and cathodic sections give rise to β_a, β_c values. The inhibition efficiency (IE%) from i_{corr} values was calculated based on eqn. 3 [26]:

$$IE\ (\%) = \frac{i_{corr(blank)} - i_{corr(inhibited)}}{i_{corr(blank)}} \times 100 \quad (3)$$

where $i_{corr\ (blank)}$ and $i_{corr\ (inhibited)}$ denotes the corrosion current densities in the absence and presence of inhibitor, respectively.

Surface analysis: The experimental results were verified by the surface analysis. The post-exposure studies were performed after 6 h immersion of the mild steel in 1 N H_2SO_4 without and with 10 ppm SPH at 303 K. The metal specimens once removed from the test media were rinsed with water, dried and subjected to various surface analysis. The morphology and the elemental composition of metal surface is investigated through scanning electron microscopy (energy-dispersive X-ray spectroscopy) SEM-EDXS. The surface wettability tests were performed using water contact angle measuring system to assess the protective film formed. The topography of the exposed metal was evaluated three-dimensionally by atomic force microscopy (AFM). The Fourier transform infrared spectroscopy (FTIR) was studied in the range 4000-500 cm^{-1} using the Perkin-Elmer Inc. Instrument (Akron, USA) and confirmed the inhibitor interaction with the metal surface. Raman spectroscopy analyses the nature of the corrosion products formed upon exposure to the acidic medium.

RESULTS AND DISCUSSION

Weight loss method: The corrosion rates and the inhibitory effect of silk protein hydrolysate (SPH) concentrations (1, 2, 4, 8 and 10 ppm) at 303 K were evaluated using mass-loss measurements. The results emphasize SPH to serve as a potent inhibitor functioning with an efficiency of 76.57% for low concentration of 1 ppm (Fig. 1). It is also clear that the corrosion rate decreased with substantial increment of inhibitor concentration. This could be due to the intense adsorption/increased surface coverage on the metal surface by the large number of inhibitor molecules making the aggressive acid species futile towards the corrosion process [27].

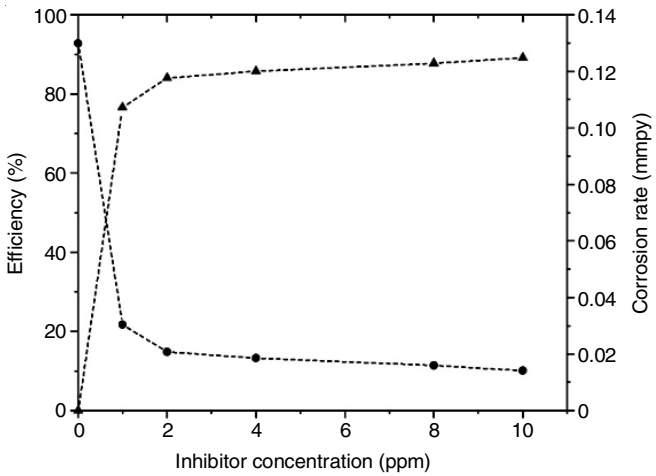

Fig. 1. Effect of different concentrations of SPH on the inhibition efficiency and corrosion rate for mild steel in 1 N H_2SO_4 at 303 K

Effect of immersion time: Fig. 2 portrays the corrosion inhibition potentials of SPH obtained for mild steel in 1 N H_2SO_4 at 303 K in various time interval for 24 h. Up to 6 h of immersion, the inhibitory impact is strong, but after that, its effectiveness sharply declines, presumably because the molecules of the inhibitor cannot withstand the prolonged exposure times. The steady increase in the protection performance until 6 h may be due to the increase in the adsorption of inhibitor onto the metal surface. Desorption of the inhibitor molecules over time explains for the gradual reduction observed subsequently.

Effect of temperature: The effect of temperatures (303, 313, 323 and 333 K) for mild steel in 1 N H_2SO_4 with SPH

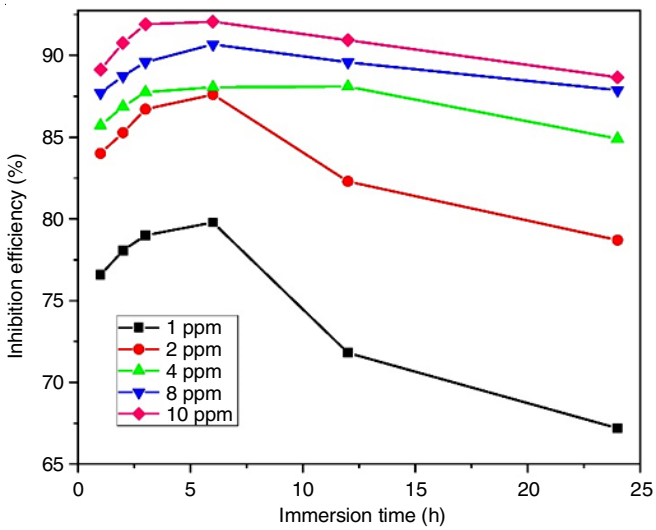

Fig. 2. Effect of immersion time on the inhibition efficiency of mild steel at different concentrations of SPH

concentrations is depicted in Fig. 3. It is obvious that the corrosion process takes place too rapidly at high temperatures owing to the rise in corrosion rate and a considerable reduction in the inhibition action. Corrosion rate increase can be attributed to a higher average kinetic energy of acid molecules, which is in excess in comparison to inhibitor metal interaction [28]. Furthermore, the desorption of adsorbed inhibitor molecules causes a decrease in inhibition efficiency at elevated temperatures due to the physical adsorption process of corrosion.

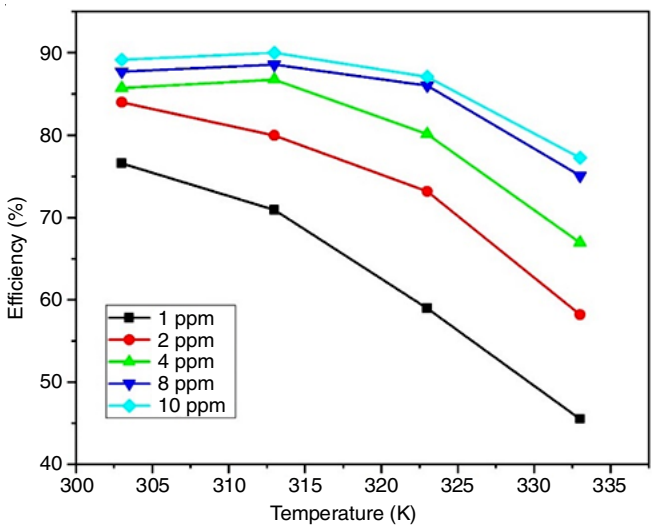

Fig. 3. Temperature effect on the inhibitor efficiency for mild steel in 1 N H_2SO_4

Thermodynamic parameters: The temperature influence over the corrosion rate can be expressed through eqn. 4, Arrhenius equation [29]:

$$\log CR = \frac{-E_a}{2.303RT} + \log A \quad (4)$$

where, CR = the corrosion rate, A = Arrhenius pre-exponential factor, E_a = the apparent activation energy, R = universal gas constant and T = absolute temperature. Fig. 4 illustrates the plot of log CR against 1000/T for different concentrations of SPH. The straight line gives slope ($-E_a/2.303R$) from which the value of E_a is determined and the values are listed in Table-1. The obtained values are higher for the inhibited system than for the uninhibited system, a characteristic of the increased energy barrier. As E_a increases, it suggests that a protective thin coating has formed on the metal surface, which is inhibiting both energy and mass transfer [30]. These findings suggest that the adsorption of SPH over the metal surface to occur through physical interactions.

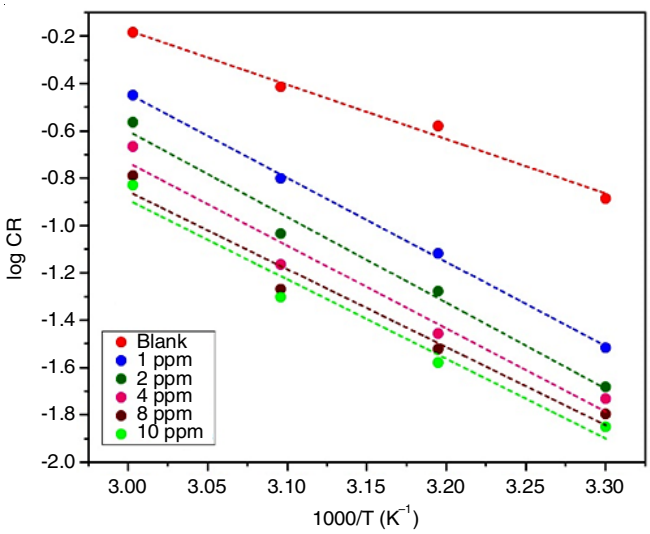

Fig. 4. Arrhenius plot for mild steel in 1 N H_2SO_4 in the absence and presence of SPH

TABLE-1
THERMODYNAMIC PARAMETERS OF MILD STEEL IN 1 N H_2SO_4 WITH AND WITHOUT DIFFERENT CONCENTRATIONS OF SPH

Inhibitor conc. (ppm)	E_a (KJ mol^{-1})	ΔH° (KJ mol^{-1})	ΔS° (KJ^{-1} mol^{-1})	E_a–ΔH°
Blank	43.88	41.25	-125.48	2.6
1	67.98	65.35	-58.30	2.6
2	69.41	66.78	-57.04	2.6
4	67.10	64.47	-66.52	2.6
8	63.02	60.39	-81.07	2.6
10	64.29	61.66	-77.95	2.6

The heat of adsorption (ΔH°) and entropy of adsorption (ΔS°) values are supportive in understanding the adsorption mechanism of inhibitor at the metal/solution interface. The values were evaluated using eqn. 5 [31]:

$$\log CR = \frac{RT}{Nh}\exp\frac{\Delta S^\circ}{R}\exp-\frac{\Delta H^\circ}{RT} \quad (5)$$

where, h is the Planck's constant and N is the Avogadro's number. Fig. 5 represents the plot of log CR/T *vs.* 1000/T with slope ($-\Delta H^\circ/2.303R$) and intercept [log R/Nh + ($\Delta S^\circ/2.303R$)], respectively. The positive values of ΔH° (Table-1) concludes the endothermic nature of mild steel dissolution in the presence of inhibitor. The E_a values were found to be higher than ΔH°, a consequence of the corrosion process involving a gaseous reaction. Additionally, it obeys the equation $E_a - \Delta H^\circ = RT$, a

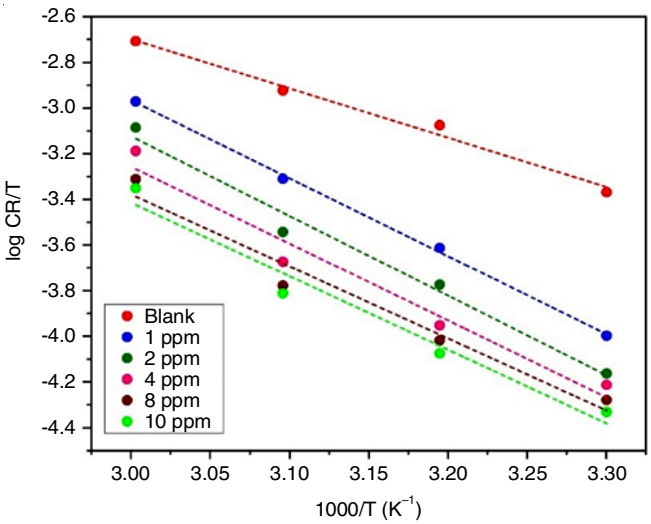

Fig. 5. Transition plot for mild steel in 1 N H_2SO_4 in the absence and presence of SPH

representative of the unimolecular corrosion process [32]. The large negative entropy values were apparent of decrease in the disorderness on moving from the inhibitor SPH to its adsorbed form [33-35].

Adsorption isotherm: The adsorption isotherm is helpful in simulating the appropriate adsorptive interaction occurring at the electrode/electrolyte interface. Selecting the appropriate adsorption isotherm model is based on the exact correlation coefficients (R^2) and linear fits. The experimental outcome confirmed the adsorption of SPH on the mild steel surface to follow Langmuir isotherm, which is expressed by eqn. 6 [36]:

$$\frac{C}{\theta} = \frac{1}{K_{ads}} + C \quad (6)$$

where, C is the inhibitor concentration, θ is the surface coverage and K_{ads} is the adsorptive equilibrium constant, respectively. The K_{ads} values were calculated from the Langmuir isotherm plots as displayed in Fig. 6. The standard free energy of adsorption (ΔG°) data is computed using eqn. 7 [37]:

$$\Delta G^\circ = -RT \ln (55.5\ K_{ads}) \quad (7)$$

The numeral 55.5 represents the water concentration in acidic solution. The value of ΔG° is associated with the type of interaction possibly to occur between SPH molecules and the mild steel surface. Its values up to -20 KJ mol^{-1} is indicative of electrostatic attraction between the charged amino acid units and the metal surface (physisorption), while the values between -20 and -40 KJ mol^{-1} is associated with sharing of charges between SPH molecules and metal surface (chemisorption) [38]. The ΔG° values (Table-2) suggested that the physisorption process is likely involved in the interaction. The large values of K_{ads} at low temperatures signifies an efficient inhibitor-metal interaction offering higher inhibition efficiencies. But their low values at higher temperatures suggested that the inhibitor has a modest effect on the metal surface [39,40].

TABLE-2
ADSORPTION PARAMETERS OBTAINED FROM LANGMUIR ISOTHERM PLOT

Temp. (K)	Slope	K_{ads}	R^2	ΔG°
303	1.1	4.91	0.9999	-14.12
313	1.0	3.08	0.9999	-13.38
323	1.0	1.67	1.0000	-12.17
333	1.1	0.93	0.9997	-10.92

Potentiodynamic polarization: The polarization plots observed for mild steel in 1 N H_2SO_4 without and with increasing dosages of SPH are shown in Fig. 7. The parameters inferred from anodic and cathodic Tafel profiles are listed in Table-3. The observations clearly indicated that with the addition of inhibitor, the polarization curves displaced slightly towards noble potentials with lower corrosion current densities. Accordingly, the E_{corr} value shows a maximum displacement of 36 mV with regard to blank, suggesting SPH to behave as a mixed type inhibitor [41]. Furthermore, the presence of inhibitor also lowers the magnitude of i_{corr}, which consecutively reduces the corrosion rates. The formation of the barrier film is also evident from the decrease in corrosion rate with increasing inhibitor

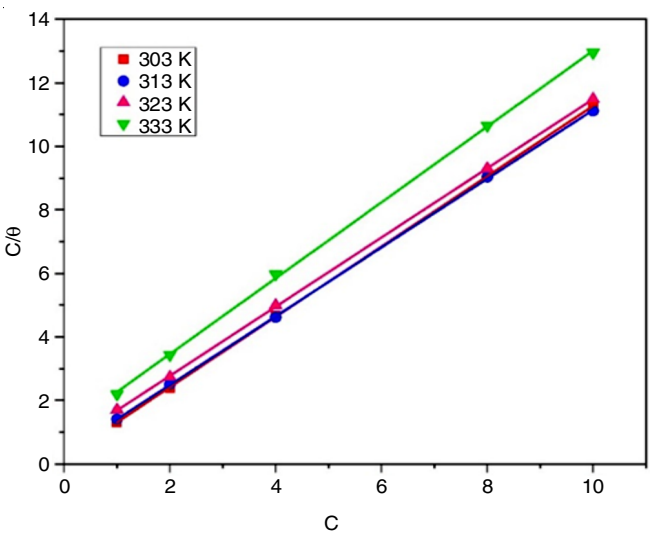

Fig. 6. Langmuir adsorption isotherm plot of SPH for mild steel corrosion in 1 N H_2SO_4 at 303 K

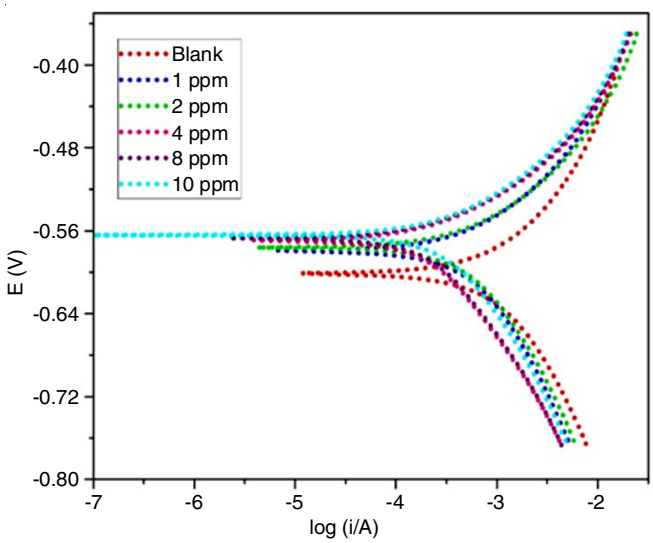

Fig. 7. Potentiodynamic Polarization curves for mild steel in one normal sulphuric acid with different concentrations of SPH at 303 K

TABLE-3
ELECTROCHEMICAL PARAMETERS OBTAINED FROM POLARIZATION PLOTS FOR MILD STEEL IN 1 N H_2SO_4 BEFORE AND AFTER TREATMENT WITH INHIBITOR

Inhibitor conc. (ppm)	E_{corr} (V)	i_{corr} (mA cm^{-2})	β_a (V dec^{-1})	β_c (V dec^{-1})	CR (mpy)	RP (Ω)	IE (%)
Blank	-0.6003	1.2730	7.015	5.161	1937.0	28	–
1	-0.5793	0.5659	11.040	6.041	861.2	45	55.54
2	-0.5760	0.5155	12.487	6.702	784.5	44	59.50
4	-0.5688	0.3423	12.738	6.756	520.9	65	73.11
8	-0.5676	0.2299	16.173	7.348	349.9	80	81.94
10	-0.5643	0.2234	16.348	7.380	339.9	82	82.45

strengths. No significant difference is noticed with the trend of β_a and β_c values, suggesting the inhibitors to function by blocking mechanism at the metal sites minimizing both metal dissolution and hydrogen evolution [42,43]. An abrupt increase in polarization resistance R_p owes to the enhanced inhibitor adsorption thereby restricting/lowering metal corrosion reaction [44,45].

Surface analysis

SEM studies: Fig. 8a displays the SEM micrograph of mild steel dipped in 1 N H_2SO_4. The bare metal looks highly damaged with severe cracks activated by the aggressive media. However, the metal immersed in inhibited acid exhibits a smooth surface (Fig. 8b), which is symbolic of the existence of protective layer formed by the reactive entities in SPH

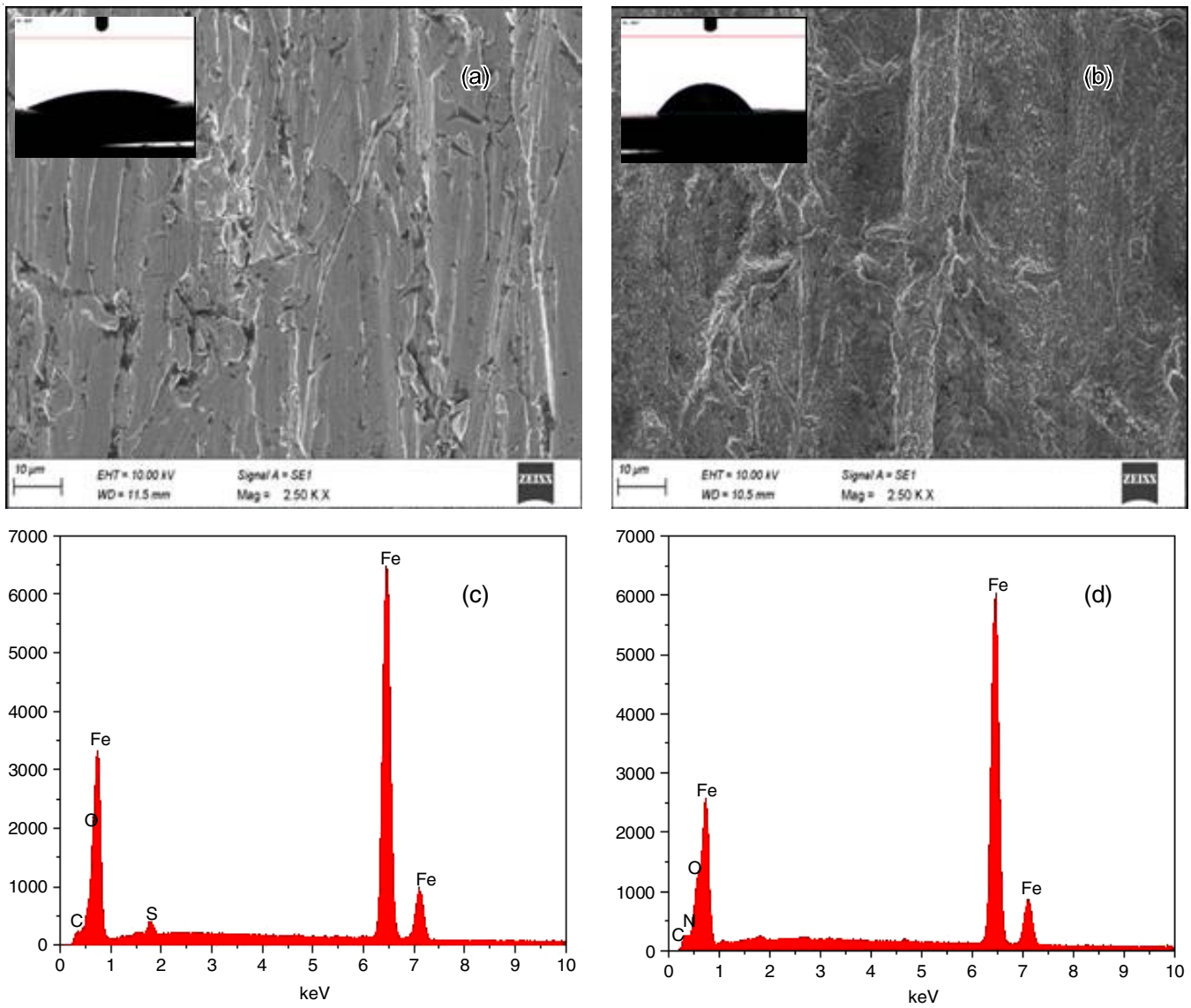

Fig. 8. SEM micrographs (a & b), EDS spectra (c & d) recorded for of mild steel after 6 h immersion in 1 N H_2SO_4 before and after treatment with the 10 ppm SPH

offering the protection against acid attack. The EDXS spectra recorded for the selected regions of SEM images are shown in Fig. 8c-d. The spectrum obtained for the mild steel submerged in acidic solution shows peak for Fe and O, indicating the occurrence of iron oxide/hydroxide on the metal surface under study [46]. On other hand, the reduction in the atomic percentage of iron and oxygen in presence of inhibitor ensures a decrease in the number of corrosion active sites [47]. The low amounts of oxygen together with the peak spotted for nitrogen in the EDXS spectra in presence of SPH validates the active adsorption of inhibitor molecules to the metal surface and these results are consistent with the observations of elemental mapping (Fig. 9). Moreover, the surface functionality of the inhibitor is witnessed through water contact angle (WCA) measurement. For the mild steel in the inhibitor-free acid, the contact angle was found to be 22.8º. This low value is associated with the hydrophilic character, a resultant of the corrosion products formed which are polar in nature. However, the value increased to 64.4º with 10 ppm SPH concentration, this imparts considerable hydrophobic property to the mild steel surface which blankets the metal from the corrosive attack [48].

Atomic force microscopic (AFM) studies: The topography of the mild steel at nano to micro-scale level provide the inhibition ability of the studied inhibitor. Fig. 10a-b highlights the 3D images of uninhibited and inhibited mild steel surface. The evaluation shows average roughness (S_a) value of 176.75 nm diminished to 120.53 nm with 10 ppm SPH. However, the metal exposed to inhibitor possess a uniform coverage of inhibitor molecules, which hinders the movement of the corrosive species onto the surface and supress the rate of corrosion leading to reduce the surface roughness [49].

FT-IR studies: The FT-IR spectra of SPH and corrosion products formed on the metal surface is shown in Fig. 11. This evaluation assists in identifying the active units of the inhibitor responsible for adsorption on the metal surface. The peak at 1638.56 cm^{-1} is ascribed to the carbonyl stretch, the frequency at 1529.74 cm^{-1} corresponds to N-H bend, the O-H and C-N stretch are observed at 3256.07 and 1114.63 cm^{-1}. The spectrum of mild steel after exposure for 6 h in 1 N H_2SO_4 containing 10 ppm SPH exhibits frequency at 1654.92, 1427.32, 3385.07 and 1028.04 cm^{-1} for C-O, N-H, O-H and C-N, respectively. These shifts in intensities indicated the interaction between the SPH molecules with the mild steel surface. Most importantly, the peaks shifted to a lower frequency range might greatly interact with the mild steel surface. The absorption in the lower region, peak at 705.94 corresponds to Fe-O/Fe-N interactions [50].

Raman studies: The results of Raman spectroscopy for the mild steel after 6 h exposure in 1 N H_2SO_4 and with 10 ppm SPH are shown in Fig. 12a-b. The strong bands at 227, 290, 402, 496, 605 cm^{-1} are apparent with the occurrence of hematite (α-Fe_2O_3) and the peak at 1300 cm^{-1} was identified as lepidocrocide (γ-FeOOH) [51,52]. The peak intensities of the corrosion products decreased remarkably under inhibitor's influence as

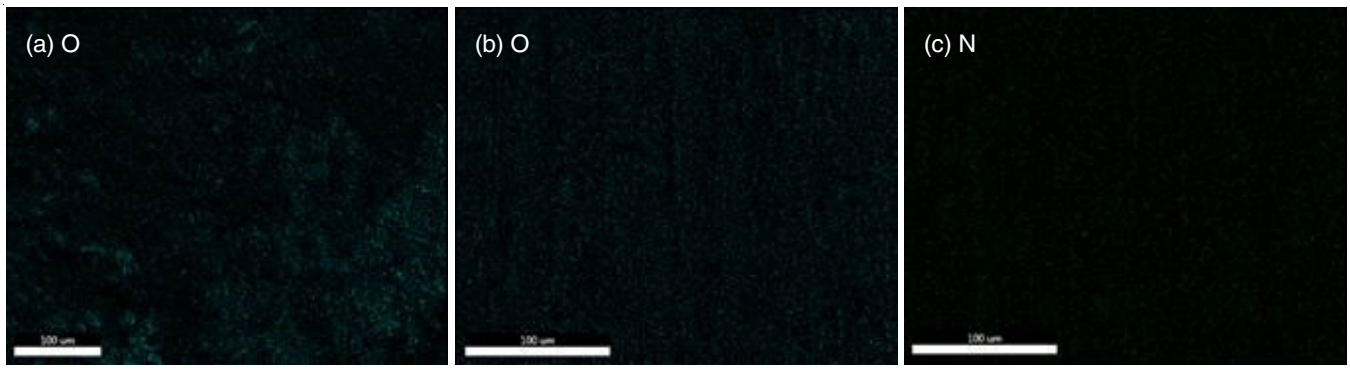

Fig. 9. EDXS elemental mapping of mild steel surface after 6 h immersion in 1 N H_2SO_4 (a), 1 N H_2SO_4 + 10 ppm SPH (b & c)

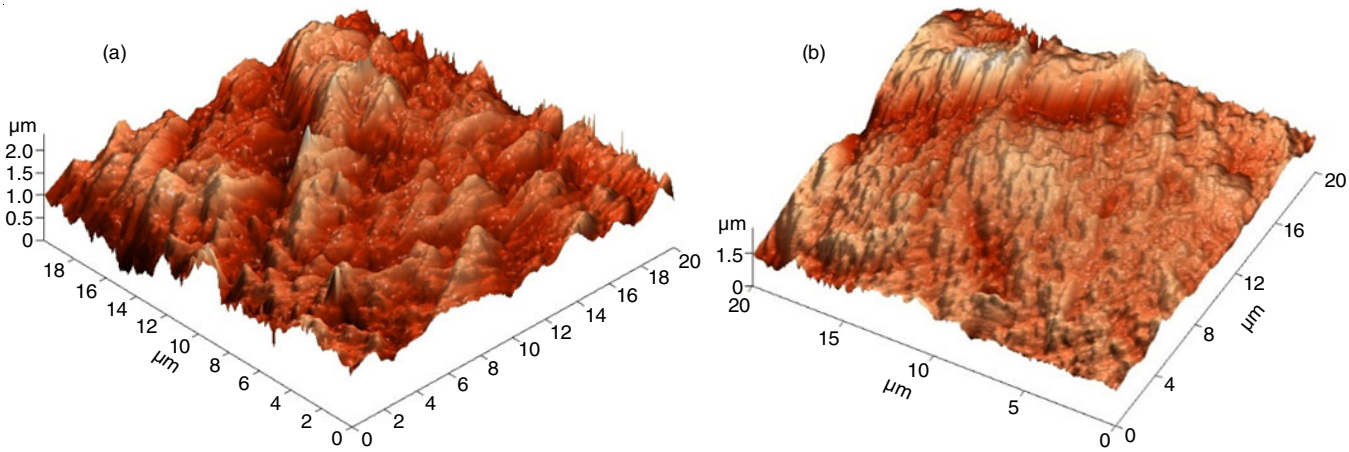

Fig. 10. AFM images of mild steel immersed in 1 N H_2SO_4 (a) without SPH (b) with SPH

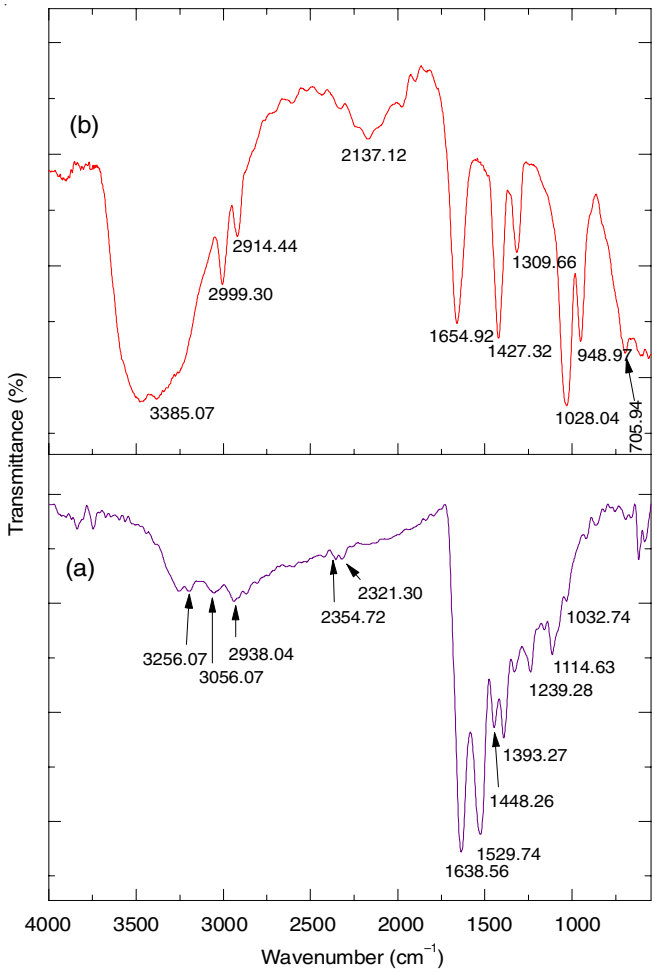

Fig. 11. FT-IR spectrum of (a) SPH (b) mild steel surface in 1 N H_2SO_4 + 10 ppm SPH

illustrated in Fig. 12b. Furthermore, the Raman shifts observed in contrast with that of the blank can be attributed to the adsorption of amino acid units directly on the mild steel surface/on the surface of the adsorbed corrosion products.

Corrosion inhibition: The amino acid moieties of SPH exist as protonated species in acidic medium and gets adsorbed at the more reactive anodic sites preventing the escape of metal ions into the solution. The adsorption of these cationic forms is favoured by the SO_4^{2-} ions present in the acid medium [53]. A weak electrostatic interaction prevails between the charged inhibitor and metal surface, this enables the resistive layer formation. The nitrogen and oxygen atoms present in the functional groups –NH_2, –COOH, –OH are greatly responsible for the coordination with the metal surface forming an inhibitive film. Of which, nitrogen is expected to contribute the maximum towards adsorption with mild steel surface which is consistent with results of EDXS analysis and the IR shifts of N-H, C-N to the lower frequency validates the point.

However, aspartic acid, glutamic acid, serine and glycine are the major constituents of SPH, offering a greater hand in the initial adsorption process. Moreover, with increasing inhibitor concentrations, the other amino acid molecules in SPH together with the aforementioned major constituents are expected to participate in the adsorption process possibly because of the van der Waals force of attraction between the amino acid units.

The intermolecular hydrogen bonding must be the reason for these forces of attraction between the inhibitor molecules, which is evident from the IR band observed at 3385.07 cm^{-1}. With longer immersion times, the number of hydrogen bonding also increases which add strength to the initially adsorbed layer, resembling an increasing close pack film acting as a thick barrier preventing the metal dissolution. The formation of the thick barrier also restricts the penetration of H^+ ions near to that of mild steel surface and reduces the hydrogen evolution. The higher E_a values in inhibitor's presence also confirms the increased energy barrier, a resultant of weak electrostatic interaction of the inhibitor's adsorption with the mild steel surface.

The developed network of intermolecular hydrogen bonding might be the major cause for the higher inhibition efficiency up to 6 h immersion at 303 K. Furthermore, with the elevation in temperature, the hydrogen bonding becomes

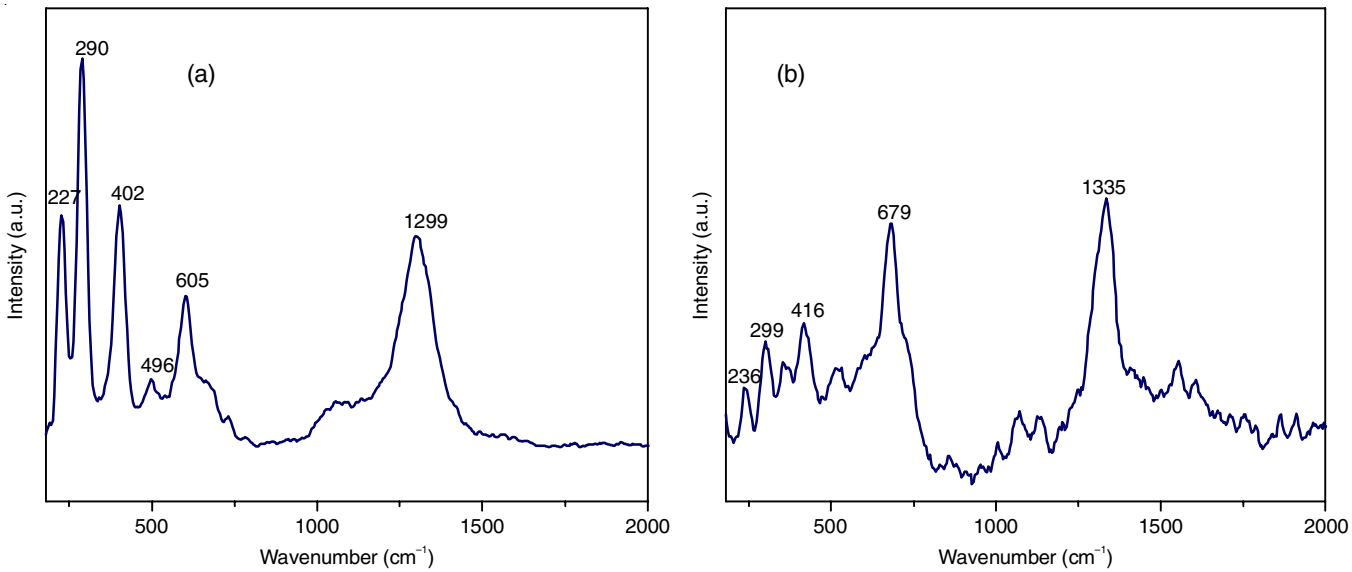

Fig. 12. Raman spectra of mild steel surface in 1 N H_2SO_4 (a) without 10 ppm SPH (b) with 10 ppm SPH

relatively weak and the strength of the adsorbed inhibitor layer decreases. Finally, the passage of the corrosive species *via* the layers of adsorption corrodes the metal surface and reduces the inhibition performance.

Although, literature presents numerous studies involving amino acids as inhibitors for mild steel [54-57]. Yet superior efficiencies are observed only for higher levels of inhibitor concentrations. Evidently, the present investigation concludes silk protein hydrolysate (SPH) to be a potent inhibitor for mild steel in H_2SO_4 medium for its remarkable efficiency values at low concentrations of 10 ppm. Importantly and interestingly, such inhibitions might have strictly arisen from the combined effect of the amino acids present in SPH.

Conclusion

The outcome of the study suggests that the silk protein hydrolysate (SPH) as an efficient inhibitor functioning at low concentrations. A maximum efficiency of 92.07% was observed for 10 ppm concentration at 303 K for 6 h immersion. The inhibition performance increases with increase in SPH concentration and decreases with rise in temperature. The results obtained from the weight loss measurements and polarization studies were in accordance. The magnitude of Gibb's free energy of adsorption confirmed the inhibition mechanism to occur predominantly through physisorption following Langmuir isotherm. The surface examination studies confirmed the adsorptive film formed over the mild steel surface.

CONFLICT OF INTEREST

The authors declare that there is no conflict of interests regarding the publication of this article.

REFERENCES

1. F. Marhamati, M. Mahdavian and S. Bazgir, *Sci. Rep.*, **11**, 18374 (2021); https://doi.org/10.1038/s41598-021-97944-7
2. S. Ibrahim, R. Sanmugapriya, J.A. Selvi, T.P. Malini, P.A. Vivekanand, P. Kamaraj, G. Periyasami, A. Aldalbahi, K. Perumal, J. Madhavan and S. Khanal, *Int. J. Photoenergy*, **2022**, 7276670 (2022); https://doi.org/10.1155/2022/7276670
3. L.F. Li, P. Caenen and J.P. Celis, *Corros. Sci.*, **50**, 804 (2008); https://doi.org/10.1016/j.corsci.2007.09.006
4. O.S.I. Fayomi and A.P.I. Popoola, *J. Phys.: Conf. Ser*., **1378**, 022006 (2019); https://doi.org/10.1088/1742-6596/1378/2/022006
5. P. Mourya, S. Banerjee, R.B. Rastogi and M.M. Singh, *Ind. Eng. Chem. Res.*, **52**, 12733 (2013); https://doi.org/10.1021/ie4012497
6. B. Thirumalairaj and M. Jaganathan, *Egyptian J. Petroleum*, **25**, 423 (2016); https://doi.org/10.1016/j.ejpe.2015.09.002
7. S.A. Umoren, U.M. Eduok, M.M. Solomon and A.P. Udoh, *Arab. J. Chem.*, **9**, S209 (2016); https://doi.org/10.1016/j.arabjc.2011.03.008
8. D. Vishnu and B. Dhandapani, *Curr. Anal. Chem.*, **17**, 260 (2021); https://doi.org/10.2174/1573411016666200110090607
9. N. Al Otaibi and H.H. Hammud, *Molecules*, **26**, 7024 (2021); https://doi.org/10.3390/molecules26227024
10. V. Soni, P. Raizada, P. Singh, H. N. Cuong, Rangabhashiyam S., A. Saini, R.V. Saini, Q.V. Lee, A.K. Nadda, T.-T.Le and V.-H. Nguyen, *Environ. Res.*, **202**, 111622 (2021); https://doi.org/10.1016/j.envres.2021.111622
11. B.F. Zehra, A. Said, H.M. Eddine, E. Hamid, H. Najat, N. Rachid and L.I. Toumert, *J. Mol. Struct.*, **1259**, 132737 (2022); https://doi.org/10.1016/j.molstruc.2022.132737
12. L.K.M.O. Goni, M.A.J. Mazumder, S.A. Ali, M.K. Nazal and H.A. Al-Muallem, *Int. J. Miner. Metall. Mater.*, **26**, 467 (2019); https://doi.org/10.1007/s12613-019-1754-4
13. A. Kasprzhitskii, G. Lazorenko, T. Nazdracheva and V. Yavna, *Computation*, **9**, 1 (2020); https://doi.org/10.3390/computation9010001
14. A.A. Farag, A.S. Ismail and M.A. Migahed, *Egyptian J. Petroleum*, **27**, 1187 (2018); https://doi.org/10.1016/j.ejpe.2018.05.001
15. T. Rabizadeh and S.K. Asl, *J. Mol. Liq.*, **276**, 694 (2019); https://doi.org/10.1016/j.molliq.2018.11.162
16. R. Menaka and S. Subhashini, *J. Adhes. Sci. Technol.*, **30**, 1622 (2016); https://doi.org/10.1080/01694243.2016.1156382
17. K. Vimal and R.B.V. Appa, *New J. Chem.*, **41**, 6278 (2017); https://doi.org/10.1039/C7NJ00553A
18. V. Pokhmurskyi, Ì.M. Zin', Ì.B. Tymus', S.À. Kornii, Î.V. Karpenko, Î.P. Khlopyk and N.I. Korets'ka, *Mater. Sci.*, **55**, 522 (2020); https://doi.org/10.1007/s11003-020-00334-z
19. L. Hamadi, S. Mansouri, K. Oulmi and A. Kareche, *Egypt. J. Petroleum*, **27**, 1157 (2018); https://doi.org/10.1016/j.ejpe.2018.04.004
20. P. Roy, T. Maji, S. Dey and D. Sukul, *RSC Adv.*, **5**, 61170 (2015); https://doi.org/10.1039/C5RA12266J
21. B. El Ibrahimi, A. Jmiai, L. Bazzi and S. El Issami, *Arab. J. Chem*., **13**, 740 (2020); https://doi.org/10.1016/j.arabjc.2017.07.013
22. G.A. Miguel and C. Álvarez-López, *Braz. J. Food Technol.*, **23**, e2019058 (2020); https://doi.org/10.1590/1981-6723.05819
23. C. Bungthong, C. Wrigley, T. Sonteera and S. Siriamornpun, *Molecules*, **26**, 3455 (2021); https://doi.org/10.3390/molecules26113455
24. M.T. Saeed, M. Saleem, S. Usmani, I.A. Malik, F.A. Al-Shammari and K.M. Deen, *J. King Saud Univ. Sci.*, **31**, 1344 (2019); https://doi.org/10.1016/j.jksus.2019.01.013
25. T.A. Salman, Q.A. Jawad, M.A.M. Hussain, A.A. Al-Amiery, L.M. Shaker, A.A.H. Kadhum and M.S. Takriff, *Cogent Eng.*, **7**, 1826077 (2020); https://doi.org/10.1080/23311916.2020.1826077
26. S.S. Durodola, A.S. Adekunle, L.O. Olasunkanmi and J.A.O. Oyekunle, *Electroanalysis*, **32**, 2693 (2020); https://doi.org/10.1002/elan.202060227
27. D. Parajuli, S. Sharma, H.B. Oli, D.S. Bohara, D.P. Bhattarai, A.P. Tiwari and A.P. Yadav, *Electrochem.*, **3**, 416 (2022); https://doi.org/10.3390/electrochem3030029
28. O.A. Akinbulumo, O.J. Odejobi and E.L. Odekanle, *Resul. Materials*, **5**, 100074 (2020); https://doi.org/10.1016/j.rinma.2020.100074
29. M.R. Laamari, J. Benzakour, F. Berrekhis, A. Derja and D. Villemin, *Arab. J. Chem.*, **9**, S245 (2016); https://doi.org/10.1016/j.arabjc.2011.03.018
30. I.A. Annon, A.S. Abbas, W.K. Al-Azzawi, M.M. Hanoon, A.A. Alamiery, W.N.R.W. Isahak and A.A.H. Kadhum, *S. Afr. J. Chem. Eng.*, **41**, 244 (2022); https://doi.org/10.1016/j.sajce.2022.06.011
31. K. Muthamma, P. Kumari, M. Lavanya and S.A. Rao, *J. Bio Tribocorros.*, **7**, 10 (2021); https://doi.org/10.1007/s40735-020-00439-7
32. H.S. Gadow and M. Fakeeh, *RSC Adv.*, **12**, 8953 (2022); https://doi.org/10.1039/D2RA01296K
33. A. Ostovari, S.M. Hoseinieh, M. Peikari, S.R. Shadizadeh and S.J. Hashemi, *Corros. Sci.*, **51**, 1935 (2009); https://doi.org/10.1016/j.corsci.2009.05.024
34. E.E. Ebenso and I.B. Obot, *Int. J. Electrochem. Sci.*, **5**, 978 (2010).
35. M. Rbaa, M. Galai, A.S. Abousalem, B. Lakhrissi, M.E. Touhami, I. Warad and A. Zarrouk, *Ionics*, **26**, 503 (2020); https://doi.org/10.1007/s11581-019-03160-9
36. X. Zheng, M. Gong, Q. Li and L. Guo, *Sci. Rep.*, **8**, 9140 (2018); https://doi.org/10.1038/s41598-018-27257-9

37. M. Tezeghdenti, L. Dhouibi and N. Etteyeb, *J. Bio Tribocorros.*, **1**, 16 (2015); https://doi.org/10.1007/s40735-015-0016-x
38. C. Verma, M.A. Quraishi, M. Makowska-Janusik, L.O. Olasunkanmi, K. Kluza and E.E. Ebenso, *Sci. Rep.*, **7**, 44432 (2017); https://doi.org/10.1038/srep44432
39. A. Saxena, K.K. Thakur and N. Bhardwaj, *Surf. Interfaces*, **18**, 100436 (2020); https://doi.org/10.1016/j.surfin.2020.100436
40. A.E.A.S. Fouda, A.H. El-Askalany, A.F.S. Molouk, N.S. Elsheikh and A.S. Abousalem, *Sci. Rep.*, **11**, 21672 (2021); https://doi.org/10.1038/s41598-021-00701-z
41. E.B. Caldona, M. Zhang, G. Liang, T.K. Hollis, C.E. Webster, D.W. Smith Jr. and D.O. Wipf, *J. Electroanal. Chem.*, **880**, 114858 (2021); https://doi.org/10.1016/j.jelechem.2020.114858
42. L. Fragoza-Mar, O. Olivares-Xometl, M.A. Domínguez-Aguilar, E.A. Flores, P. Arellanes-Lozada and F. Jiménez-Cruz, *Corros. Sci.*, **61**, 171 (2012); https://doi.org/10.1016/j.corsci.2012.04.031
43. M. Parveen, M. Mobin and S. Zehra, *RSC Adv.*, **6**, 61235 (2016); https://doi.org/10.1039/C6RA10010D
44. M.M. Saleh, *Mater. Chem. Phys.*, **98**, 83 (2006); https://doi.org/10.1016/j.matchemphys.2005.08.069
45. Z.P. Mathew, K. Rajan, C. Augustine, B. Joseph and S. John, *Heliyon*, **6**, e05560 (2020); https://doi.org/10.1016/j.heliyon.2020.e05560
46. M. Goyal, H. Vashisht, A. Kumar, S. Kumar, I. Bahadur, F. Benhiba and A. Zarrouk, *J. Mol. Liq.*, **316**, 113838 (2020); https://doi.org/10.1016/j.molliq.2020.113838
47. A. Chaouiki, M. Chafiq, H. Lgaz, M.R. Al-Hadeethi, I.H. Ali, S. Masroor and I.-M. Chung, *Coatings*, **10**, 640 (2020); https://doi.org/10.3390/coatings10070640
48. K. Xhanari, N. Grah, M. Finšgar, R. Fuchs-Godec and U. Maver, *Chem. Pap.*, **71**, 81 (2017); https://doi.org/10.1007/s11696-016-0046-y
49. M. Nasibi, M. Mohammady, E. Ghasemi, A. Ashrafi, D. Zaarei and G. Rashed, *J. Adhes. Sci. Technol.*, **27**, 1873 (2013); https://doi.org/10.1080/01694243.2013.764144
50. V.R. Palayoor, J.T. Kakkassery, S.S. Kanimangalath and S. Varghese, *Int. J. Ind. Chem.*, **8**, 49 (2017); https://doi.org/10.1007/s40090-016-0101-0
51. P. Colomban, S. Cherifi and G. Despert, *J. Raman Spectrosc.*, **39**, 881 (2008); https://doi.org/10.1002/jrs.1927
52. T.D. Manh, T.L. Huynh, B.V. Thi, S. Lee, J. Yi and N.N. Dang, *ACS Omega*, **7**, 8874 (2022); https://doi.org/10.1021/acsomega.1c07237
53. F. Bentiss, M. Lagrenée and M. Traisnel, *Corrosion*, **56**, 733 (2000); https://doi.org/10.5006/1.3280577
54. J. Fu, S. Li, Y. Wang, L. Cao and L. Lu, *J. Mater. Sci.*, **45**, 6255 (2010); https://doi.org/10.1007/s10853-010-4720-0
55. M. Mobin, M. Parveen and M.A. Khan, *Recent Res. Sci. Technol.*, **3**, 40 (2011).
56. K. Zhang, W. Yang, X. Yin, Y. Chen, Y. Liu, J. Le and B. Xu, *Carbohydr. Polym.*, **181**, 191 (2018); https://doi.org/10.1016/j.carbpol.2017.10.069
57. A. Toghan, A. Fawzy, N. Alqarni, A. Abdelkader and A.I. Alakhras, *Int. J. Electrochem. Sci.*, **16**, 1 (2021); https://doi.org/10.20964/2021.11.40